suspension. It is likely that only a small portion of the DML is entrained and that the retardation one observes by chromatography is observable only when it is magnified by the long column bed. In a highly viscous DNA solution (>10 P) the DML diffusion rate is slowed to only 3.5×10^{-7} cm^2/sec. This compares with a diffusion rate of $D = 1.8 \times 10^{-8}$ cm^2/sec for spin-labeled phosphatidylcholine in vesicles (Devaux and McConnell, 1972) and $D = 1 \times 10^{-8}$ cm^2/sec for spin-labeled steroid molecules in dipalmitoyllecithin vesicles (Träuble and Sackmann, 1972). In the DNA solution, the water diffusion rate is undiminished compared with the rate in just buffer. Apparently the DNA forms a network through which water can move unhindered but which entrains the relatively large liposomes.

The decay curve for DML in buffer reproducibly shows a biphasic decay (Figure 3) which could be interpreted in terms of two diffusion processes, one having a fast rate compared with the other. One explanation for this behavior is that the diffusion is partially restricted. At the short times one sees the unrestricted diffusion of DML within a small volume of space. At longer times the DML encounters barriers which impede the migration of the DML from that unit of space. This point deserves further investigation.

Conclusion

The diffusion of DML in solution is controlled primarily by the translational diffusion of whole liposomes. Translation of individual molecules appears to be a much slower process. One might expect therefore that the diffusion of lipids in biological membranes would be slower than 10^{-7} cm^2/sec.

References

Chapman, D., and Morrison, A. (1966), *J. Biol. Chem. 241,* 5044.

Cooper, V. G., Yedgor, S., and Barenholz, Y. (1974), *Biochim. Biophys. Acta 363,* 86.

Devaux, P., and McConnell, H. M. (1972), *J. Am. Chem. Soc. 94,* 4475.

Horwitz, A. F., Klein, M. P., Michaelson, D. M., and Cohler, S. J. (1973), *Ann. N.Y. Acad. Sci. 222,* 468.

Huang, C. (1969), *Biochemistry 8,* 344.

Huang, C., and Lee, L. (1973), *J. Am. Chem. Soc. 95,* 234.

James, T. L., and McDonald, G. G. (1973), *J. Magn. Reson. 11,* 58.

Kornberg, R. G., and McConnell, H. (1971), *Proc. Natl. Acad. Sci. U.S.A. 68,* 2564.

Lee, A. G., Birdsall, N. J. M., and Metcalfe, J. C. (1973), *Biochemistry 12,* 1650.

McLaughlin, A. C., McDonald, G. G., and Leigh, J. S., Jr. (1973), *J. Magn. Reson. 11,* 107.

Morrisett, J. D., Gallagher, J. G., Aune, K. C., and Gotto, A. M., Jr. (1974), *Biochemistry 13,* 4765.

Träuble, H., and Sackmann, E. (1972), *J. Am. Chem. Soc. 94,* 4499.

Free Energy and the Kinetics of Biochemical Diagrams, Including Active Transport†

Terrell L. Hill

ABSTRACT: In earlier papers on muscle contraction it was found very useful to relate the actual (not standard) free energy levels of the different states in the biochemical diagram of the myosin cross-bridge to the first-order rate constants governing transitions between these states and to the details of the conversion of ATP free energy into mechanical work. This same approach is applied here to other macromolecular biochemical systems, for example, carriers in active transport, and simple enzyme reactions. With the definition of free energy changes between states of a diagram used here (and in the muscle papers), the rate constants of the diagram are first order, the macromolecular transitions are effectively isomeric, the equilibrium constants are dimensionless, the free energy changes are directly related to first-order rate constant ratios, and the ratio of products of forward and backward rate constants around any cycle of the diagram is related to operational free energy changes (e.g., the in vivo free energy of ATP hydrolysis). These general points are illustrated by means of particular arbitrary models, especially transport models. In contrast to the muscle case, the free energy conversion question in other biochemical systems can be handled at the less detailed, complete-cycle level rather than at the elementary transition level. There is a corresponding complete-cycle kinetics, with composite first-order rate constants for the different possible cycles (in both directions). An introductory stochastic treatment of cycle kinetics is included.

A biochemical diagram (see, e.g., Hill, 1968) shows the possible states of a system (usually a macromolecule, or macromolecular complex) as points and represents each inverse pair of possible first-order transitions between two states as a line between the corresponding points.

This paper is concerned primarily with the connections between the free energies of the states of a diagram and the first-order rate constants associated with the transitions or lines in the diagram. The discussion applies to biochemical diagrams generally but free energy transducing systems are of primary interest.

Actually, this subject was introduced, from the present

† From the Laboratory of Molecular Biology, National Institute of Arthritis, Metabolism, and Digestive Diseases, National Institutes of Health, Bethesda, Maryland 20014. *Received December 6, 1974.*

point of view, in recent papers on muscle contraction (Hill, 1974, 1975; Hill et al., 1975) where it was found very useful to relate the free energy levels of the different biochemical states of a myosin cross-bridge to the first-order rate constants governing transitions between these states and to the details of the conversion of ATP free energy into mechanical work. The possibility of applying this same approach to other biochemical systems will be pursued in the present paper using membrane transport models, primarily, as examples. However, a simple cyclic enzymatic reaction will also be discussed briefly.

The macromolecular system in the case of membrane transport is presumably a protein or protein complex, that, for convenience, we shall refer to as a "carrier" (though conformational changes rather than diffusion are generally believed to be involved in the translocation duties of carriers). A carrier embedded in a membrane is the analog of a myosin cross-bridge embedded in a myofilament structure. The carrier may exist in various biochemical states that can be connected by first-order transitions and that can be assigned corresponding relative free energy levels. Via a cycle or cycles of such states, ATP or other free energy sources can be used to produce active transport of molecules or ions across the membrane.

Several definitions of free energy changes between biochemical states are possible. The definition used for myosin states (Hill, 1974) and here for carrier states is the most helpful because of its intimate connection with the actual kinetics of the system. The rate constants are first order, the carrier transitions are effectively isomeric, the equilibrium constants are dimensionless, the free energy changes are directly related to first-order rate constant ratios and to the free energy along the reaction coordinate in the usual way, and the ratio of products of forward and backward rate constants around any cycle is related to operational free energy changes (e.g., the in vivo free energy of ATP hydrolysis). The last point places a restraint or restraints in the assignment of rate constants in any model.

In fact the essential characteristic of a system, to which the just summarized free energy and rate constant formalism of the present paper should be applied, is that the states of the biochemical diagram can all be regarded as different states of the *same* molecule (usually macromolecule or macromolecular complex). That is, there is in such systems a certain natural asymmetry in each of the various reactions involved: the macromolecule may be considered to be the dominant species while other molecules (ligands, substrates, etc.) play a secondary role.

There is still another definition of free energy changes between states that is related to the rate of entropy production in the system. This will be the subject of a subsequent paper (with R. M. Simmons).

In the muscle problem, the biochemical state diagram (Hill, 1974) is a function of a positional variable x that locates the nearest actin attachment site relative to the myosin cross-bridge in question. From a theoretical point of view, it is this feature that leads to the introduction of mechanical force and work into the analysis and hence that makes possible an understanding of how ATP free energy is converted into mechanical work (Hill, 1974; Hill et al., 1975). The membrane transport and most other biochemical problems are much simpler in that the biochemical diagram does not depend on a variable such as x, and hence mechanical work is not involved. However, whereas only one "chemical" force (ATP hydrolysis) appears in the myosin diagram, at least two such forces must be represented in the carrier diagram in order to make free energy conversion (active transport) possible. For example, there are three chemical forces (ATP, Na^+, K^+) to contend with in the NaK-ATPase system.

The general properties of membrane transport diagrams, including methods of calculating the steady-state probabilities of the biochemical states of the diagram, the net fluxes around cycles and between neighboring states, and the connection with reciprocal relations and irreversible thermodynamics (in the nonphysiological, near-equilibrium special case), have been discussed in detail elsewhere (Hill, 1966, 1968). The present paper extends this earlier theoretical formalism by the introduction of the appropriate free energy levels of the biochemical states and through discussion of related topics such as cycle kinetics and stochastics (section 4).

We shall be concerned with general methodology here and not with the advocacy of any particular model or models. But it seems desirable to present the essential material by means of arbitrarily chosen special cases (rather than in a single general, and therefore abstract, formulation). Sections 1 and 2 are especially simple because only one chemical "force" is involved in each case.

Free Energy and Kinetics at Two Levels of Detail. A distinction that will arise as the examples are discussed in the following sections is sufficiently important to warrant advance mention here.

Free energy changes, rate constants, and the associated kinetics may be considered at the individual transition level (as already referred to above) *or at the complete cycle level.* Actually, in the muscle problem one is generally obliged to follow individual transitions for two reasons: an analysis of the conversion of chemical free energy into mechanical work requires attention to single transitions; and the transition probabilities (rate constants) of the diagram are functions of a spatial variable x which itself varies linearly with time in steady contractions. But in active transport (and other biochemical problems) the transition probabilities are constant and the required free energy conversion book-keeping is related to completed cycles only and not to individual transitions within cycles. Thus, in these problems, besides considering individual states and transitions *within* each cycle, as an alternative one can work at a level somewhat less detailed. That is, one can deal with *composite* transition probabilities for completion of each kind of cycle in the diagram, in either direction, together with the overall free energy changes associated with entire cycles. This latter approach is of course closely related to the use of conventional thermodynamic *net* fluxes and forces for the system (Hill, 1968), but we shall also discuss, in an introductory way, a more novel feature, namely, the stochastics of cycle completions (section 4). Incidentally, in previous work (Hill, 1974, 1975; Hill et al., 1975) we have already emphasized the significance of a stochastic treatment of individual transitions within the diagram of biochemical states of myosin cross-bridges. The stochastics of complete cycles was also found useful (Hill, 1975) in a limiting case (very slow contractions).

1. Model for Facilitated Diffusion

We begin with the simple and well-known model in Figure 1 for the facilitated diffusion of a ligand (O) between bath A and bath B (e.g., interior and exterior of a cell or vice versa) across a membrane with the aid of a carrier that

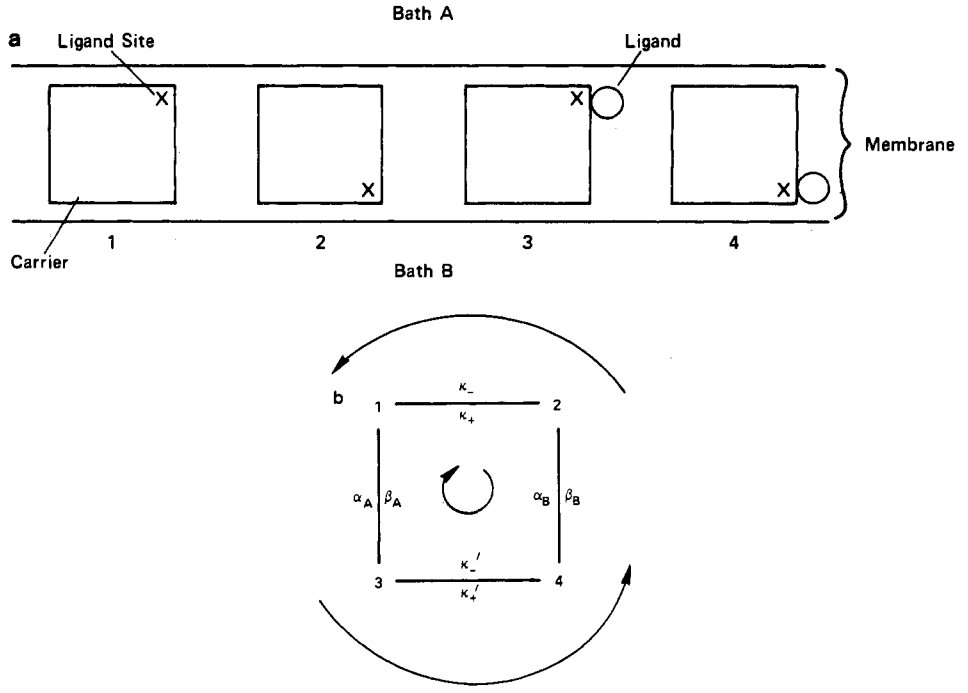

FIGURE 1: (a) Four-state model for facilitated diffusion of ligand (circle) by carrier (square). (b) Diagram showing rate constant notation. The arrows indicate applicable transition direction for rate constants.

has a single binding site (X) for a ligand molecule. There are N independent and equivalent carriers in the membrane sample. Each carrier may exist in four different states, indicated very schematically in Figure 1a. The actual mechanism of translocation across the membrane (conformational change, rotation, etc.) need not be specified.

A single carrier is a small thermodynamic system (Hill, 1963, 1964) with a Helmholtz free energy A_i when in state i (the Gibbs free energy $G_i \simeq A_i$, since the pV_i term is negligible). The bound ligand is of course included in A_3 and A_4 (Figure 1a). The discussion of a myosin cross-bridge as a small system, and its free energy, on pp 270–272 and 277–278 of Hill (1974), is largely applicable to a carrier as well.

We ignore the possibility of a charged ligand and a membrane potential at the outset but return to this topic at the end of the section.

The biochemical diagram is a single cycle in this case, shown in Figure 1b. The rate constants are first-order rate constants for transitions between carrier states with ligand at its actual molar concentrations c_A and c_B in the two baths. That is, α_A (and possibly β_A) will depend on the value of c_A while α_B (and possibly β_B) will depend on c_B. We would generally expect, in fact, $\alpha_A \sim c_A$ and $\alpha_B \sim c_B$, but this is not the only possibility (Hill et al., 1975; see also Appendix 2 of Hill, 1975). The condition for equilibrium (when $c_A = c_B$) is $\alpha_A\kappa_+'\beta_B\kappa_- = \alpha_B\kappa_-'\beta_A\kappa_+$. Otherwise there is a steady state (we do not consider transients) with a mean net flux $\bar{J}$ around the cycle (Figure 1b) corresponding to net transport of ligand across the membrane. The explicit expression for $\bar{J}$ in the direction A $\rightarrow$ B is (Hill, 1966, 1968)

$$\bar{J} = \frac{N(\alpha_A\kappa_+'\beta_B\kappa_- - \alpha_B\kappa_-'\beta_A\kappa_+)}{\alpha_A\kappa_+'\beta_B + \text{15 similar terms}} \quad (1)$$

We denote the steady-state probability of state i by p_i and the equilibrium value by p_i^e. Of course $\Sigma_i p_i = 1$. Also, the chemical potential of ligand in the two baths is

$$\mu_A = \mu^0 + kT \ln c_A$$
$$\mu_B = \mu^0 + kT \ln c_B, \quad (2)$$

where μ^0 = standard free energy and we understand c to mean (molar) activity rather than concentration, if necessary. At equilibrium, $\mu_A = \mu_B$. Otherwise $\mu_A - \mu_B$ is the thermodynamic force driving ligand from bath A to bath B.

With the actual bath concentrations c_A and c_B, we now consider, for example, transitions $1 \rightleftarrows 3$ with all other transitions in the cycle imagined blocked. Consideration of the resulting equilibrium between states 1 and 3 will allow us to relate A_1 and A_3 to α_A and β_A. The standard free energy change for the process

$$\text{ligand} + \text{carrier 1} \rightleftharpoons \text{carrier 3} \quad (3)$$

has the conventional relationship to the equilibrium quotient:

$$A_3 - (\mu^0 + A_1) = -kT \ln (p_3^e/p_1^e c_A) \quad (4)$$

But we want to pursue especially the alternative "isomeric" point of view, $1 \rightleftarrows 3$, instead of eq 3. The isomeric detailed balance relation is $\alpha_A p_1^e = \beta_A p_3^e$. On rearranging eq 4, we can write

$$\frac{p_3^e}{p_1^e} = \frac{\alpha_A}{\beta_A} = \exp\left\{-\frac{[A_3 - (\mu_A + A_1)]}{kT}\right\} \quad (5)$$

This is the isomeric equilibrium quotient. Although eq 4 and 5 are essentially equivalent, eq 5 shows that *first-order* rate constants are related to the *actual* free energy change (at c_A) of real interest rather than to the standard free energy change (at $c_A = 1\ M$) in eq 4.

In writing eq 4 and 5 we appealed to conventional thermodynamics without a formal proof. The same result follows from statistical mechanics (pp 278 and 325–327 of Hill, 1974; see also eq 7–9 of Hill, 1960 where $q = Q_3/Q_1$, $Q_3 = e^{-A_3/kT}$, etc., $\theta = p_3^e$, and $1 - \theta = p_1^e$).

Now if the imaginary blocks in the rest of the cycle are removed, a steady state will be reached with state probabilities p_i. But the rate constants and free energies in eq 5 re-

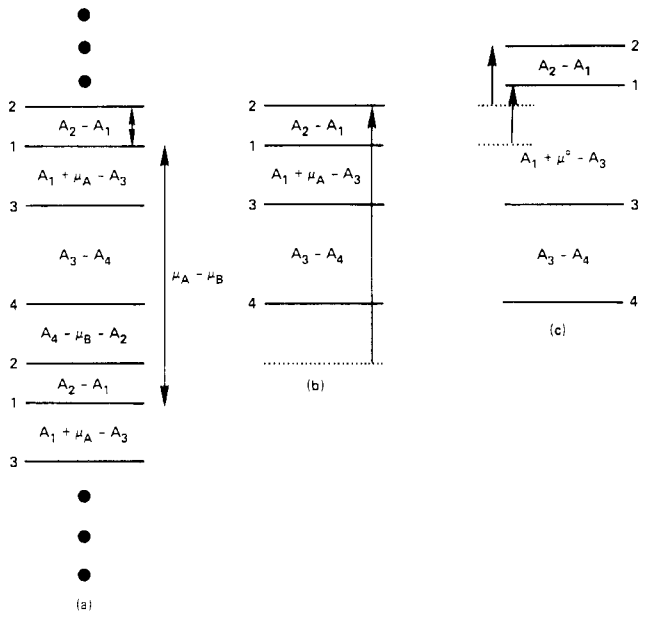

FIGURE 2: (a) Illustrative infinite set of steady-state free energy levels for model in Figure 1. (b) Set of free energy levels in special case of equilibrium. (c) Set of standard free energy levels.

main unaltered. Thus the second equality in eq 5, between rate constants and free energies, is a general relation and still holds even though the first equality does not (i.e., steady-state probabilities do not satisfy detailed balance relations).

Note that if c_A is varied in eq 5, μ_A and α_A/β_A are affected but not $A_3 - A_1$.

We can, of course, *define* an isomeric equilibrium constant $K_{13} \equiv \alpha_A/\beta_A$ that has, according to eq 5, the usual relationship to a free energy change, in this case to the *actual* free energy change $A_3 - (\mu_A + A_1)$. K_{13} is dimensionless.

By a similar argument we also find for the rest of the cycle

$$K_{34} = \frac{\kappa_+'}{\kappa_-'} = \exp\left[-\frac{(A_4 - A_3)}{kT}\right] \quad (6)$$

$$K_{42} = \frac{\beta_B}{\alpha_B} = \exp\left\{-\frac{[(\mu_B + A_2) - A_4]}{kT}\right\} \quad (7)$$

$$K_{21} = \frac{\kappa_-}{\kappa_+} = \exp\left[-\frac{(A_1 - A_2)}{kT}\right] \quad (8)$$

These introduce the remaining actual free energy changes between carrier states. On multiplying eq 5-8 together, we obtain

$$K_{13}K_{34}K_{42}K_{21} = \frac{\alpha_A\kappa_+'\beta_B\kappa_-}{\alpha_B\kappa_-'\beta_A\kappa_+} = e^{(\mu_A - \mu_B)/kT} \quad (9)$$

The quantity $\mu_B - \mu_A = kT \ln (c_B/c_A)$ is the *total* or net actual free energy change associated with one counterclockwise cycle (a ligand molecule is transported from bath A to bath B). Each of the three members of eq 9 is equal to unity only at equilibrium ($c_A = c_B$, $\mu_A = \mu_B$). When $\mu_A > \mu_B$, these members are greater than unity, there is a net free energy drop of magnitude $\mu_A - \mu_B$ with each counterclockwise cycle, and there is a mean net counterclockwise flux (ligand: A → B), given by eq 1.

For contrast, it is worth repeating the above analysis using standard free energy changes, as in eq 4. We introduce second-order rate constants α_A' and α_B' defined by $\alpha_A = \alpha_A'c_A$ and $\alpha_B = \alpha_B'c_B$. The detailed balance equation related to eq 4 is $\alpha_A'c_Ap_1^e = \beta_Ap_3^e$. Then

$$\frac{\alpha_A'}{\beta_A} \equiv K_{13}' = \exp\left\{-\frac{[A_3 - (\mu^0 + A_1)]}{kT}\right\} \quad (10)$$

In similar fashion, we find

$$\frac{\beta_B}{\alpha_B'} \equiv K_{42}' = \exp\left\{-\frac{[(\mu^0 + A_2) - A_4]}{kT}\right\} \quad (11)$$

Equations 6 and 8 are unchanged. The analog of eq 9 is then

$$K_{13}'K_{34}K_{42}'K_{21} = \frac{\alpha_A'\kappa_+'\beta_B\kappa_-}{\alpha_B'\kappa_-'\beta_A\kappa_+} \equiv 1 \quad (12)$$

since the total *standard* free energy change for one complete cycle is zero. This also follows from eq 9 if we put $c_A = c_B = 1$ (hence $\mu_A = \mu_B = \mu^0$). These properties obtain whether the system is at steady state or at equilibrium; hence they are not very informative.

Figure 2a shows a possible illustrative set of steady-state free energy levels (or, rather, free energy differences since only these are significant), corresponding to eq 5-8, for the carrier states in Figure 1. In this example, we have chosen $\mu_A > \mu_B$ (and $c_A > c_B$) and there is a free energy drop in each counterclockwise step of the cycle (this need not be the case but the figure is thereby simplified). Each free energy difference is related to a first-order rate constant quotient (eq 5-8). Because each step has been assigned a free energy drop, each of these rate constant quotients is greater than unity. The overall free energy drop per counterclockwise cycle is $\mu_A - \mu_B$. The set of free energy levels 13421 is repeated indefinitely above and below those levels shown in the figure, one set for each cycle.

From a stochastic point of view, at the individual transition level, a carrier performs a biased one-dimensional walk on the free energy levels of Figure 2a. The transition probabilities governing the walk are the first-order rate constants. The bias is in favor of downward transitions, as determined by the free energy differences (eq 5-8). The net flux (A → B) contributed by a single carrier is equal to the net number of completed downward cycles (13421). For further details, see Hill (1975), section VI.

An *equilibrium* special case is shown in Figure 2b. In this case we start with the steady state represented by Figure 2a, hold c_A (and μ_A) constant, but increase c_B (and μ_B) until $c_B = c_A$. The result is the *single* set of equilibrium free energy levels in Figure 2b. The dotted level 2 (from Figure 2a) is raised by an amount $\mu_A - \mu_B$ (the three other free energy differences are unchanged) so that now the overall free energy change in the cycle 13421 is zero. The quotient β_B/α_B in eq 7 is now much less than unity. The relative populations (p_i^e) of the four carrier states now follow a Boltzmann distribution ($p_4^e > p_3^e > p_1^e > p_2^e$), as determined by the three free energy differences (Figure 2b). This is *not* true of the steady-state populations (p_i) and levels in Figure 2a (for an explicit example, see pp 330-331 of Hill (1974)).

Figure 2c illustrates a possible set of *standard* free energy levels, related to second-order rate constants as in eq 10 and 11. The differences $A_2 - A_1$ and $A_3 - A_4$ are unchanged. We suppose in this example that $c_A = c_B < 1\ M$ in Figure 2b. Hence both levels 1 and 2 in Figure 2b (dotted in Figure 2c) must be raised by the same amount relative to 3 and 4 to arrive at Figure 2c, because the standard state has higher concentrations, $c_A = c_B = 1\ M$. There is again only a single set of free energy levels in Figure 2c since this is an "equilibrium" situation ($c_A = c_B$).

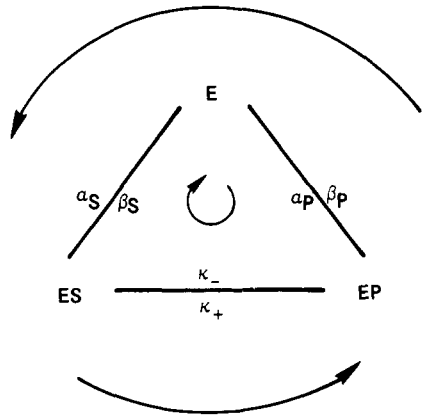

FIGURE 3: Diagram for reaction S → P catalyzed by enzyme. The arrows indicate applicable transition direction for rate constants.

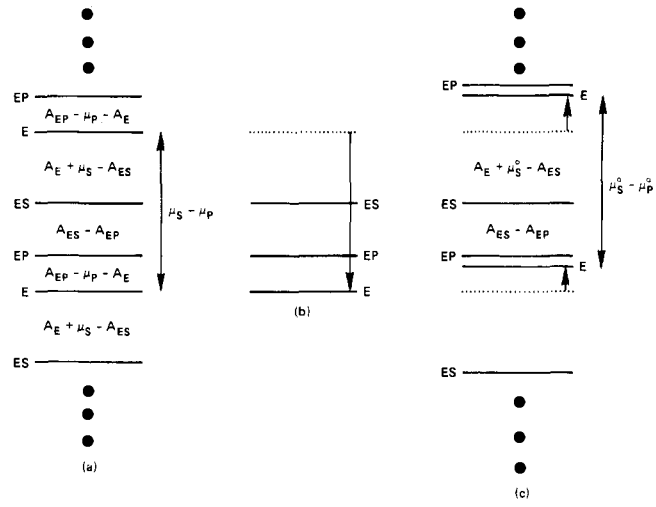

FIGURE 4. (a) Illustrative set of steady-state free energy levels for diagram in Figure 3. (b) Equilibrium special case. (c) Illustrative set of standard free energy levels.

The relative standard free energy levels in Figure 2c and the rate constant ratios in eq 6, 8, 10, and 11 are an invariant set (independent of the actual values of c_A and c_B). In contrast, for example, the free energy difference between states 4 and 2 and the value of the ratio β_B/α_B associated with Figure 2a change continuously to values appropriate to Figure 2b as c_B is increased from its initial value (Figure 2a) to its final value $c_B = c_A$ (Figure 2b).

Invariance, of course, always has a certain appeal. But in this case it is a disadvantage. The *actual* free energy levels (and corresponding first-order rate constants) must be used in order to follow the time course of the free energy of this steady-state system (rate of net free energy dissipation; efficiency of free energy conversion; in maximum detail, the stochastics of the free energy changes in the system).

Incidentally, it should be mentioned that, in the case of a "reduced" diagram (Hill, 1975; Hill et al., 1975), α_A' and β_A might both vary with c_A though α_A'/β_A is constant (similarly for α_B' and β_B). Thus the invariance referred to above need not extend to the individual rate constants.

Suppose ligand and/or carrier are charged and that the two baths have different electrostatic potentials ψ_A and ψ_B. There will be a varying electrostatic potential ψ inside the membrane. Whichever bath represents the outside of the cell is usually chosen to be the zero of potential. The terms $ze\psi_A$ and $ze\psi_B$ must now be added to eq 2 to give the electrochemical potentials μ_A and μ_B, respectively, where ϵ = charge on proton, and z = charge number of ligand (e.g., +1 for Na^+). Each carrier free energy A_i will now include a similar term for each of its charges (including bound ligand) but using the local ψ at each charge. Equilibrium occurs when $\mu_A = \mu_B$. Thus, isomeric equations such as eq 5-9 remain unchanged in appearance and have the same physical significance. But to retain the same standard chemical potential μ^0 in the two baths and the equilibrium condition $c_A = c_B$, we must now understand the symbol c_A to include a factor $e^{ze\psi_A/kT}$ and c_B to include $e^{ze\psi_B/kT}$ (recall that c_A and c_B are already understood to include activity coefficients where necessary). This convention leaves all of our discussion and notation above intact, but it is, of course, an arbitrary convention adopted merely to avoid rewriting equations. It will be understood in the remainder of the paper without further mention.

2. Model for Enzyme-Substrate Reaction

This brief section is a digression from the main membrane-transport theme of this paper. But it introduces in a simple way another important class of applications of these free energy considerations.

First, to emphasize the analogy with immobile (embedded) cross-bridges and carriers, we consider independent and equivalent enzyme molecules E that are adsorbed on a surface or embedded in one side of a membrane, and that are in contact with a single solution (bath) that contains both substrate molecules S and product molecules P. We consider later the alternate case in which the enzyme molecules are free to move about in the solution.

Figure 3 shows the three-state cycle or diagram, which is conventional except for the (first-order) rate constant notation. The chemical potentials of S and P are

$$\begin{aligned} \mu_S &= \mu_S^0 + kT \ln c_S \\ \mu_P &= \mu_P^0 + kT \ln c_P \end{aligned} \tag{13}$$

We consider only stationary states with the "free" concentrations c_S and c_P independent of time. When $\mu_S > \mu_P$, the enzyme catalyzes steady turnover of S into P. The flux $\bar{J}$ can be expressed in the same form as eq 1 (Hill, 1966, 1968; Mahler and Cordes, 1971, eq 6-54).

Corresponding to eq 5-9, we have here, in obvious notation,

$$K_1 \equiv \frac{\alpha_S}{\beta_S} = \exp\left\{-\frac{[A_{ES} - (\mu_S + A_E)]}{kT}\right\} \tag{14}$$

$$K_2 \equiv \frac{K_+}{K_-} = \exp\left[-\frac{(A_{EP} - A_{ES})}{kT}\right] \tag{15}$$

$$K_3 \equiv \frac{\beta_P}{\alpha_P} = \exp\left[-\frac{[(\mu_P + A_E) - A_{EP}]}{kT}\right] \tag{16}$$

$$K_1K_2K_3 = \frac{\alpha_S K_+ \beta_P}{\alpha_P K_- \beta_S} = e^{(\mu_S - \mu_P)/kT} \tag{17}$$

The quantity $\mu_P - \mu_S$ is the free energy change (usually negative) associated with one counterclockwise cycle (one S at c_S is converted to one P at c_P). The equilibrium case is $\mu_S = \mu_P$ (all three members of eq 17 are equal to unity).

Figure 4a shows a hypothetical (infinite) set of free energy differences for this system (again each counterclockwise step is chosen arbitrarily to show a free energy drop). The first-order rate constants of any model of this type imply a set of free energy levels, as in eq 14-16 and Figure 4a.

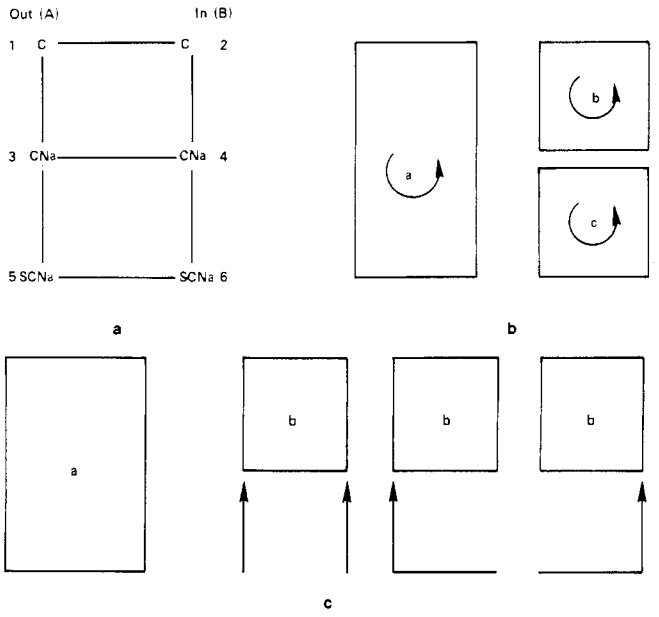

FIGURE 5: (a) Diagram for active transport of substrate S by Na^+ via carrier C. (b) Cycles of the diagram. Arrows indicate choice of positive flux direction. (c) Flux diagrams for cycles a and b. Cycle c is similar to cycle b.

Equation 17 imposes a restraint on the rate constants chosen for the model since $\mu_S - \mu_P$ is generally a known quantity. An example is S = ATP and P = ADP + P_i, where $\mu_S - \mu_P$ is of the order of 10–12 kcal mol^{-1}.

Figure 4b shows an equilibrium case. Here we start with Figure 4a, hold c_P and μ_P constant, and decrease c_S and μ_S until $\mu_S = \mu_P$. The result is a single set of three equilibrium free energy levels. Correspondingly, $p_E^e > p_{EP}^e > p_{ES}^e$ (Boltzmann distribution).

If we use standard free energies μ_S^0 and μ_P^0 in eq 14–16, we must also introduce K_1', K_3', α_S', and α_P' (see eq 10 and 11). Then eq 17 becomes

$$K_1'K_2K_3' = \frac{\alpha_S'\kappa_+\beta_P}{\alpha_P'\kappa_-\beta_S} = e^{(\mu_S^0-\mu_P^0)/kT} \qquad (18)$$

The three members of this equation are not equal to unity as in eq 12 (or, at equilibrium, as in eq 17), but they are independent of c_S and c_P. Figure 4c shows a possible infinite (and invariant) set of standard free energy differences constructed from Figure 4a (dotted lines in Figure 4c) on the assumption that both $c_S < 1\ M$ and $c_P < 1\ M$ in Figure 4a (whereas, in Figure 4c, $c_S = c_P = 1\ M$). The free energy drop in one cycle is $\mu_S^0 - \mu_P^0$; this is not the actual free energy drop.

Now let us consider this same system with the enzyme molecules in solution. This serves as a very simple prototype for models based on the action of embedded enzymes (e.g., in myofilaments or membranes) that are extracted from their natural habitats and investigated in homogeneous solution (the homogeneity, incidentally, removes the possibility of "directional" free energy conversion—as occurs in both muscle contraction and membrane transport). In the homogeneous myosin–actin–ATP system, actin must be treated as an additional ligand. The model with Figure 3 extended by inclusion of another ligand (that effects the enzyme kinetics) will be discussed in the subsequent paper with R. M. Simmons.

We can use the same first-order rate constant notation as in Figure 3, though of course one expects in general that all six rate constants (especially α_S and α_P) would be somewhat different in the "free enzyme" case as compared with "immobilized enzyme" (above).

The solution is assumed to be dilute in E, ES, and EP so that the enzyme molecules behave independently of each other. Their chemical potentials in solution can be written

$$\mu_E = \mu_E^0 + kT \ln c_E \qquad (19)$$

and similarly for ES and EP. In the binding equilibrium E + S $\rightleftarrows$ ES (at c_S) considered by itself (as in eq 3–5)

$$\begin{gathered}\mu_E + \mu_S = \mu_{ES} \\ \mu_{ES}^0 - (\mu_S^0 + \mu_E^0) = -kT \ln (c_{ES}^e/c_E^e c_s)\end{gathered} \qquad (20)$$

The (first-order) detailed balance relation is now $\alpha_S c_E^e = \beta_S c_{ES}^e$. Thus, corresponding to eq 5, we have

$$\frac{c_{ES}^e}{c_E^e} = \frac{\alpha_S}{\beta_S} = \exp\left\{-\frac{[\mu_{ES}^0 - (\mu_S + \mu_E^0)]}{kT}\right\} \qquad (21)$$

This is as far as we need carry the analysis. We see that the difference $A_{ES} - A_E$ for an immobilized enzyme (eq 14) is merely replaced by $\mu_{ES}^0 - \mu_E^0$ for a free enzyme (compare Hill, 1963, section 2-3). The same is true in eq 15 and 16. Equations 17 and 18 are unchanged. Thus free energy levels of enzyme states, as in Figure 4a, that correspond to the actual concentrations c_S and c_P and that are related as before to first-order rate constants, can still be used even if the enzyme molecules are in solution. The total concentration of enzyme is immaterial so long as the solution is dilute in enzyme (i.e., each enzyme molecule is kinetically independent). The free energy change $\mu_{ES}^0 - (\mu_S + \mu_E^0)$ is the desired *actual* free energy change per enzyme molecule for S (at c_S) + E $\rightarrow$ ES, as before (eq 14), despite the appearance of standard chemical potentials for E and ES. This is because the effect of the choice of standard state is cancelled on taking the *difference* $\mu_{ES}^0 - \mu_E^0$. There will always be such a difference and cancellation in systems of this type.

3. Model for Active Transport Caused by Concentration Gradient

In this model (Figure 5a) a ligand S (e.g., a sugar or amino acid) is transported across a membrane from outside (bath A) to inside (bath B) by a carrier (C) that must be activated by Na^+ binding before ligand can be bound. This is a well-known model; the transitions 3 $\rightleftarrows$ 4 (Figure 5a) are often omitted. The case of primary interest occurs when the downhill Na^+ electrochemical gradient (out $\rightarrow$ in) is large enough to drive the ligand uphill (out $\rightarrow$ in) against its concentration gradient. That is, in obvious notation,

$$\begin{gathered}\Delta\mu_{Na} \equiv \mu_{Na}^{out} - \mu_{Na}^{in} > 0 \\ \Delta\mu_S \equiv \mu_S^{out} - \mu_S^{in} < 0\end{gathered} \qquad (22)$$

$$\Delta\mu_{Na} > -\Delta\mu_S \qquad (23)$$

There are thus *two* thermodynamic (chemical) forces operating in this model.

If the mean net fluxes (out $\rightarrow$ in) are denoted by $\bar{J}_{Na}$ and $\bar{J}_S$ (both positive in the usual case), then the efficiency of free energy conversion is obviously

$$\eta = -\bar{J}_S\Delta\mu_S/\bar{J}_{Na}\Delta\mu_{Na} \quad 0 \le \eta \le 1 \qquad (24)$$

while the rate of entropy production is

$$T\dot{S}_i = \bar{J}_{Na}\Delta\mu_{Na} + \bar{J}_S\Delta\mu_S \geq 0 \qquad (25)$$

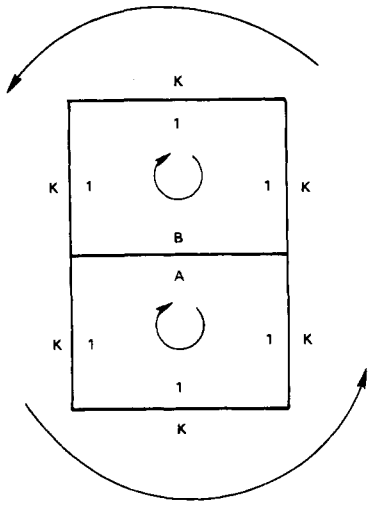

FIGURE 6: Special choice of rate constants for diagram in Figure 5.

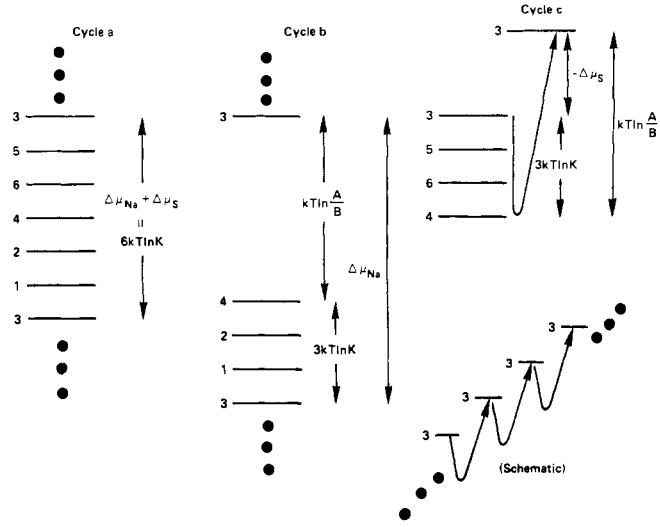

FIGURE 7: Illustrative sets of free energy levels for diagram in Figure 6, using $A/B = K^{5.5}$. See text for further details.

Equations 24 and 25 apply to steady states arbitrarily far from equilibrium (the near-equilibrium situation and the related irreversible thermodynamics are of theoretical but not of physiological interest).

Seven pairs of first-order rate constants are implicit in the diagram, Figure 5a (compare Figures 1b and 3), and we denote them by α_{ij} (for $i \rightarrow j$), using the number assignment of states shown in the figure. The diagram has three cycles (Figure 5b), with mean net counterclockwise fluxes denoted by $\bar{J}_a, \bar{J}_b, \bar{J}_c$. Clearly

$$\begin{aligned} \bar{J}_{Na} &= \bar{J}_a + \bar{J}_b \\ \bar{J}_S &= \bar{J}_a + \bar{J}_c \end{aligned} \tag{26}$$

The method of obtaining explicit expressions for $\bar{J}_a$, $\bar{J}_b$, and $\bar{J}_c$ from the rate constants of the diagram (compare eq 1), in terms of flux diagrams, is given in detail in Hill (1966, 1968). Figure 5c shows the flux diagrams for cycles a and b; by symmetry, cycle c also has three flux diagrams.

We can again define isomeric equilibrium constants K_{13}, K_{34}, etc., by first-order rate constant ratios, just as in eq 5-8. These are related to free energy differences by

$$K_{13} = \frac{\alpha_{13}}{\alpha_{31}} = \exp\left\{-\frac{[A_3 - (\mu_{Na}{}^{out} + A_1)]}{kT}\right\} \tag{27}$$

$$K_{34} = \frac{\alpha_{34}}{\alpha_{43}} = \exp\left[-\frac{(A_4 - A_3)}{kT}\right] \tag{28}$$

$$K_{64} = \frac{\alpha_{64}}{\alpha_{46}} = \exp\left\{-\frac{[(A_4 + \mu_S{}^{in}) - A_6]}{kT}\right\} \tag{29}$$

etc. Thus, as in sections 1 and 2, the full set of rate constants determines all of the free energy differences. If we multiply K's around each cycle (as in eq 9 and 17), we obtain

$$\text{cycle a: } K_{35}K_{56}\ldots K_{13} = \exp[\Delta\mu_{Na} + \Delta\mu_S)/kT] > 1 \tag{30}$$

$$\text{cycle b: } K_{34}\ldots K_{13} = \exp(\Delta\mu_{Na}/kT) > 1 \tag{31}$$

$$\text{cycle c: } K_{35}\ldots K_{43} = \exp(\Delta\mu_S/kT) < 1 \tag{32}$$

The rate constants (and K's) of the model must be consistent with the operational quantities on the right-hand side of these equations.

Special Case: Free Energies. In order to be able to write explicit but relatively simple illustrative equations, let us now turn to the very specialized case shown in Figure 6. In this example *all* of the counterclockwise rate constants in cycle a have the value K relative to their inverse rate constants, all of which are assigned the reference value unity. Thus all equilibrium constants in eq 30 are equal to K. The rate constants α_{34} and α_{43} (relative to the same reference value) are denoted A and B, respectively, so that $K_{34} = A/B$. Then, from eq 30-32

$$\text{a: } K^6 = \exp[(\Delta\mu_{Na} + \Delta\mu_S)/kT] > 1 \quad K > 1 \tag{33}$$

$$\text{b: } K^3(A/B) = \exp(\Delta\mu_{Na}/kT) > K^6 \tag{34}$$

$$\text{c: } K^3(B/A) = \exp(\Delta\mu_S/kT) < 1 \quad A/B > K^3 \tag{35}$$

The free energy levels for the three cycles, determined by these rate constants, are illustrated in Figure 7 (an infinite set in each case). Downward steps correspond to the counterclockwise direction in cycles a and b. The single-headed arrows show the counterclockwise direction in cycle c. Some explicit choice has to be made for $A/B > K^3$; in this figure we have used $A/B = K^{5.5}$.

The levels are equally spaced in cycle a because all K's in eq 30 are equal. Each counterclockwise circuit around this cycle transports one S and one Na^+ from outside to inside. If this is the only significant cycle (i.e., if $A \ll 1$, $B \ll 1$), $\bar{J}_{Na} = \bar{J}_S$ ("complete coupling") and $\eta = -\Delta\mu_S/\Delta\mu_{Na} = \eta_{max} = 2.5/8.5 = 0.294$. Cycle b (34213) transports Na^+ without S. Hence, to the extent that this cycle is used, it reduces the efficiency below the above (maximum) value. The free energy drop per cycle b is $\Delta\mu_{Na}$. Cycle c transports S without Na^+, but in the "wrong" direction (i.e., down the S gradient, in $\rightarrow$ out; $\bar{J}_c$ is negative). Hence this cycle also reduces η. One counterclockwise circuit (35643) around cycle c transports one S from outside to inside and *increases* the free energy by $-\Delta\mu_S$ (Figure 7).

It might be noted that, for the above free energy considerations, we need only the ratios $K/1$ and A/B and not the separate rate constants. Thus, for example, Figure 7 would be unaffected if some of the six pairs of rate constants in cycle a were $10K/10$, $0.1K/0.1$, etc.

Two-Dimensional Free-Energy Bookkeeping. If there is only one chemical force, whether there is only one (as in Figures 1b and 3) or more than one (as in Hill, 1974, Figure 26a) cycle in the diagram, a single, infinite, one-dimensional set of free energy levels suffices in order to follow the

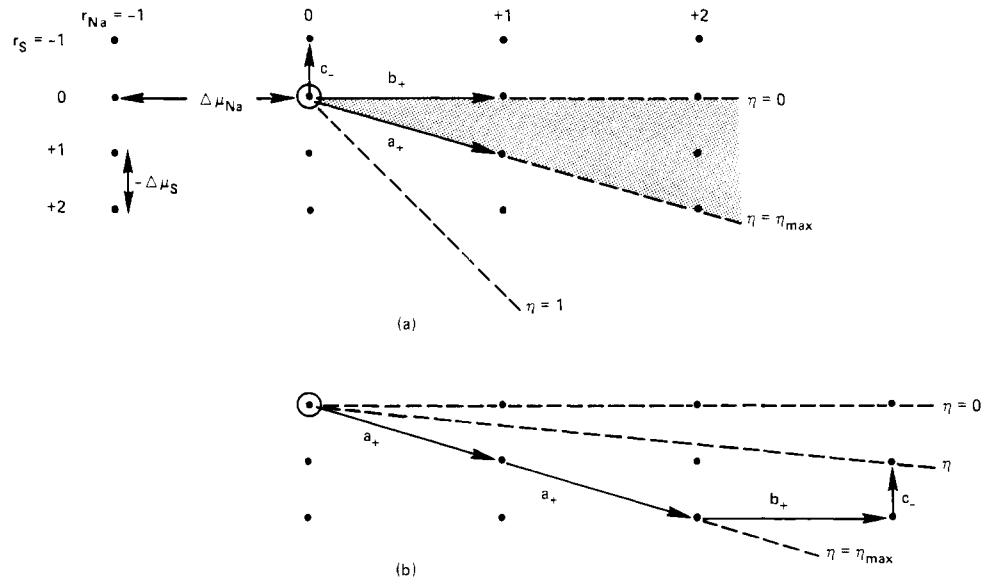

FIGURE 8: (a) Lattice for free-energy and transport bookkeeping during stochastic behavior of system in Figures 6 and 7. See text for further details. (b) Example showing efficiency η (η_{max} = 2.5/8.5 = 0.294, $\eta = \eta_{max}/3$ = 0.098).

free energy of the system (see Figures 2a and 4a here and Figure 26b in Hill, 1974). This is also sufficient if there are two or more chemical forces but only one cycle in the diagram (because of complete coupling, there is, in effect, only one *net* force; consider cycle a only, for example, in Figures 5b and 7).

However, if there are two chemical forces and more than one cycle, as in the present model, it is clear from Figure 7 that a single one-dimensional set of free energy levels is no longer adequate to monitor the free energy. Thus, Figure 7 has three sets of levels, one for each cycle, with the problem of combining the three sets left unresolved.

Fortunately, as already mentioned in the introduction, the actual free energy bookkeeping required (except when mechanical work is involved) is related to completed *cycles* only and not to individual transitions (see, for example, eq 24 and 26). For this purpose, with two chemical forces, we can use a two-dimensional free energy lattice to follow the system, as in Figure 8a. Each point in the lattice (r_S, r_{Na}) represents a *net* of r_S molecules of S and r_{Na} sodium ions transported in the direction out → in, starting, say, from $r_S = r_{Na} = 0$. The horizontal free energy unit (double-arrow) is $\Delta\mu_{Na}$ while the vertical unit is $-\Delta\mu_S$. The ratio used for $-\Delta\mu_S/\Delta\mu_{Na}$ in Figure 8a corresponds to the case in Figure 7. The three arrows emanating from the origin show, as illustrations, the lattice displacements resulting from single cycles a+, b+, and c− (+ = counterclockwise cycle,− = clockwise; see Figure 5b). Stochastically (see section 4 for further details), the system "walks" on the lattice points of Figure 8a with certain (cycle or composite) transition probabilities. At each point of such a walk, there are six possible transitions (a±, b±, c±). But over a long period of time, we will have $r_{Na} \sim \bar{J}_{Na}$ and $r_S \sim \bar{J}_S$. Also, of course, the free energy consumed is $r_{Na}\Delta\mu_{Na}$ while the free energy recovered is $r_S(-\Delta\mu_S)$, with an efficiency given by eq 24. The dashed lines in Figure 8a indicate limiting values of η: η = 1 (at 45°); $\eta = \eta_{max}$ (complete coupling, with cycle a only); and η = 0 (cycle b only). The line representing the real efficiency will lie between η = 0 and $\eta = \eta_{max}$ (shaded region). Figure 8b illustrates this for a hypothetic case in which the net cycle fluxes occur in the ratios $\bar{J}_a:\bar{J}_b:\bar{J}_c$ = 2:1:−1.

We turn next to an example (Figure 6 again) in which the three net cycle fluxes are calculated. For this purpose we must employ explicitly the *separate* rate constants in Figure 6.

Special Case: Fluxes. The routine way to derive the steady-state kinetic properties of the system in Figure 6 is, first, use directional diagrams (King and Altman, 1956; Hill, 1966, 1968) to find the probabilities $p_1, \ldots, p_6$ of the separate states in the diagram and, second, use flux diagrams (Hill, 1966, 1968), as in Figure 5c, to obtain the fluxes. In a sufficiently specialized case, such as the present one, or in a numerical example, it is actually much simpler to *reverse the procedure,* because flux diagrams are both significantly fewer in number and algebraically simpler than directional diagrams. We use the present example to illustrate this quite useful procedure which avoids the necessity of explicit consideration of directional diagrams.

The method is the following: (1) write out the flux expressions with an unknown normalization factor Σ (which is equal to the sum of all directional diagrams); (2) use the equality of fluxes between some successive steps in cycles (or the fact that the total net flux into any state is zero), expressed in terms of the p_i, to obtain $p_1\Sigma, \ldots, p_6\Sigma$; and (3) use normalization of the p_i to find Σ.

There are only seven flux diagrams for this model (Figure 5c). In contrast, there are 15 partial diagrams (Hill, 1966, 1968) and 15 × 6 = 90 directional diagrams. From the flux diagrams and Figure 6 we have immediately (Hill, 1966, 1968)

$$\begin{aligned} \bar{J}_a &= N(K^6 - 1)/\Sigma \\ \bar{J}_b &= N(AK^3 - B)(K^2 + K + 1)/\Sigma \\ \bar{J}_c &= N(BK^3 - A)(K^2 + K + 1)/\Sigma \end{aligned} \tag{36}$$

Also

$$\bar{J}_{35}/N \equiv Kp_3 - p_5 = Kp_5 - p_6 = Kp_6 - p_4 = (\bar{J}_a + \bar{J}_c)/N \tag{37}$$

and

$$\bar{J}_{42}/N \equiv Kp_4 - p_2 = Kp_2 - p_1 = Kp_1 - p_3 = (\bar{J}_a + \bar{J}_b)/N \tag{38}$$

Now we can express, say, $p_4\Sigma$ in terms of $p_3\Sigma$ from eq 36 and 37 and $p_3\Sigma$ in terms of $p_4\Sigma$ from eq 36 and 38. These two inhomogeneous linear equations can be solved for $p_3\Sigma$ and $p_4\Sigma$. The transitions $3 \rightleftarrows 4$ provide a check. The other $p_i\Sigma$ follows immediately from eq 37 and 38. Normalization then gives Σ. In this way we find

$$\begin{aligned} p_1 &= (\ )[K^3 + 1 + AK^2 + B(K + 1)]/\Sigma \\ p_2 &= (\ )[K^3 + 1 + AK(K + 1) + B]/\Sigma \\ p_3 &= (\ )[K^3 + 1 + B(\ )]/\Sigma \\ p_4 &= (\ )[K^3 + 1 + A(\ )]/\Sigma \\ p_5 &= (\ )[K^3 + 1 + A + BK(K + 1)]/\Sigma \\ p_6 &= (\ )[K^3 + 1 + A(K + 1) + BK^2]/\Sigma \end{aligned} \tag{39}$$

where

$$\begin{aligned} \Sigma &= 3(\ )[2(K^3 + 1) + (A + B)(\ )] \\ (\ ) &= K^2 + K + 1 \end{aligned} \tag{40}$$

Note that if $A = B = 0$, $p_1 = \ldots = p_6 = 1/6$, as expected. Equations 26, 36, and 40 give explicit expressions for all the fluxes.

Special Case: Numerical Example. We use here $A/B = K^4$ (not the same as in Figure 7) and $K = 2$. Thus, from eq 33 to 35, $\Delta\mu_{Na}/kT = 7 \ln K = 4.852$ (this is of the correct order of magnitude for the experimental Na^+ electrochemical gradient) and $\Delta\mu_S/kT = -\ln K = -0.6931$. Thus the maximum efficiency ($A = B = 0$) in this case is $\eta_{max} = 1/7 = 0.143$.

Table I shows state probabilities, fluxes, and the efficiency for two choices of A and B, both of which are consistent with $A/B = K^4 = 16$. The states in the table are arranged in the same order as in the diagram. On the left of the table, the A and B transitions are relatively more important than on the right. Consequently, on the left, the probabilities are less uniform, cycles b and c are used more, and the efficiency is lower. As already mentioned, if $A = B = 0$, we have all $p_i = 1/6$ and $\eta_{max} = 1/7 = 0.143$.

Table I: Example: Probabilities, Fluxes, Efficiency.

$A = 1, B = 1/16$ p_i	$A = 1/4, B = 1/64$ p_i
(1) 0.1728 (2) 0.1974	(1) 0.1686 (2) 0.1765
(3) 0.1237 (4) 0.2097	(3) 0.1529 (4) 0.1804
(5) 0.1360 (6) 0.1605	(5) 0.1568 (6) 0.1647
$\bar{J}_a/N = 0.1179$	$\bar{J}_a/N = 0.1511$
$\bar{J}_b/N = 0.1040$	$\bar{J}_b/N = 0.0333$
$\bar{J}_c/N = -0.00655$	$\bar{J}_c/N = -0.00210$
$\bar{J}_{Na}/N = 0.2219$	$\bar{J}_{Na}/N = 0.1844$
$\bar{J}_S/N = 0.1114$	$\bar{J}_S/N = 0.1490$
$\eta = 0.0717$	$\eta = 0.1154$

4. Stochastic Treatment of Cycles

The mean *net* number of completed cycles of any type, say cycle a, for any diagram and for a single system (e.g., a single carrier), after a long time t, is denoted by $\bar{r}_a$. Obviously $\bar{r}_a = \bar{J}_a t/N$. This section is concerned primarily with fluctuations in r_a about the mean value $\bar{r}_a$.

This topic was mentioned in passing in the introduction and section 3. The treatment given in this section will be simple, omitting complications. Some of these complications will be dealt with in a separate paper (Hill and Chen, 1975), using Monte Carlo numerical methods primarily.

Imagine (and this can be simulated on a computer) that we follow in detail a system, over a long period of time, as it occasionally and instantaneously changes from one state to another of its kinetic diagram, in accordance with the first-order transition probabilities of the diagram. The diagram has cycles a, b, c, ... Actually, starting in any arbitrary state, what we record as time passes is the completion of each successive cycle (the type of cycle; its direction, ±; and the time between cycles). Over an extremely long period of time, let p_{a+}, p_{a-}, p_{b+}, p_{b-}, ... be the fraction of completed cycles of type a in direction + (assigned by some convention), etc. The sum of these probabilities is unity. Also, let τ be the mean time between cycles (total time divided by the total number of cycles of any kind). Then the probability of completing any cycle in the infinitesimal interval dt is dt/τ, while the probability of completing a cycle of type a+, a−, etc., in dt is $p_{a+}dt/\tau$, $p_{a-}dt/\tau$, etc. Thus, if we denote the first-order rate constants for cycle completions by k_{a+}, k_{a-}, etc., we have $k_{a+} = p_{a+}/\tau$, $k_{a-} = p_a/\tau$, etc. These are the *composite* cycle transition probabilities already referred to in the introduction and section 3.

In an ensemble of N equivalent and independent systems (e.g., a membrane sample with N carriers), the mean numbers of cycles of each type completed per unit time are $\bar{J}_{a+} = Nk_{a+}$, $\bar{J}_{a-} = Nk_{a-}$, etc. These fluxes are always positive. The *net* cycle fluxes are then

$$\bar{J}_a = N(k_{a+} - k_{a-}) \tag{41}$$

etc. The net fluxes may be positive or negative.

The stochastic quantities introduced above may now be expressed in terms of the single-transition rate constants of the diagram. Using the diagram method (Hill, 1966, 1968), the net cycle fluxes can always be written in the form

$$\begin{aligned} \bar{J}_a &= N(\Pi_{a+} - \Pi_{a-})\Sigma_a/\Sigma \\ \bar{J}_b &= N(\Pi_{b+} - \Pi_{b-})\Sigma_b/\Sigma \end{aligned} \tag{42}$$

etc., where Σ is the sum of directional diagrams for all states, Π_{a+} is the product of rate constants around cycle a in the + direction, Π_{a-} is the product of rate constants around cycle a in the − direction, $(\Pi_{a+} - \Pi_{a-})\Sigma_a$ is the sum of cycle a flux diagrams (this defines Σ_a), etc. The expressions for Π_{a+}, Π_{a-}, Σ_a, Σ, etc., involve diagram rate constants only. Equations 1 and 36 provide examples. See pp 141-152 of Hill (1968) for a full explanation. If the diagram consists of only a single cycle (as in eq 1), eq 42 simplify to

$$\bar{J} = N(\Pi_+ - \Pi_-)/\Sigma \tag{43}$$

Equation 42a gives the mean *net* flux around cycle a. Actually, we can go further and identify $N\Pi_{a+}\Sigma_a/\Sigma$ with the mean flux around cycle a in the + direction by noting that $\bar{J}_a \to N\Pi_{a+}\Sigma_a/\Sigma$ if we let any one of the rate constants in Π_- become very small. Therefore the (composite) cycle rate constants are given explicitly by

$$\begin{aligned} k_{a+} &= \Pi_{a+}\Sigma_a/\Sigma, \\ k_{a-} &= \Pi_{a-}\Sigma_a/\Sigma \end{aligned} \tag{44}$$

etc. Note that

$$k_{a+}/k_{a-} = \Pi_{a+}/\Pi_{a-} \tag{45}$$

etc. Equation 45 can be verified in special cases by an independent "mean first passage time" type of argument based on the diagram transition probabilities. See also Hill and Chen (1975) for "experimental" confirmation.

It is interesting that the relations between individual transition rate constant ratios and actual free energy differences, as seen for example in eq 27-29, carries over to the cycle level. Thus, as a consequence of eq 45, the left-hand sides of eq 30-32 can be replaced by the cycle rate constant ratios k_{a+}/k_{a-}, k_{b+}/k_{b-}, and k_{c+}/k_{c-}, respectively. The analogy is not perfect, however, since a change of biochemical state is involved in each of eq 27-29 but completion of a cycle (eq 30-32) leaves the system unchanged (except for the transport, etc., accomplished).

There may be systems in the study of which one must be content to work, both theoretically and experimentally, entirely in terms of cycle rate constants rather than individual transition rate constants. The simplest example: for a membrane transport system with a single cycle a, radioactive tracer studies plus the net flux $\bar{J}_a$ would provide the two cycle rate constants k_{a+} and k_{a-}.

The cycle probabilities introduced above become

$$p_{a+} = \tau k_{a+} = \tau \Pi_{a+} \Sigma_a / \Sigma, \qquad p_{a-} = \tau \Pi_{a-} \Sigma_a / \Sigma \tag{46}$$

etc. Since the sum of these probabilities is unity

$$\tau = (k_{a+} + k_{a-} + k_{b+} + \ldots)^{-1} = \Sigma / (\Pi_{a+} \Sigma_a + \Pi_{a-} \Sigma_a + \Pi_{b+} \Sigma_b + \ldots) \tag{47}$$

That is, τ, the mean time between cycles, is equal to the sum of all directional diagrams divided by the sum of all flux diagrams (with all signs taken positive). The total cycle frequency for a single system of the ensemble is τ^{-1}. The cycle probabilities can also be written

$$p_{a+} = \Pi_{a+} \Sigma_a / (\Pi_{a+} \Sigma_a + \Pi_{a-} \Sigma_a + \Pi_{b+} \Sigma_b + \ldots), \tag{48}$$

etc.

Having found (eq 44) the rate constants k_{a+}, k_{a-}, k_{b+}, etc., that govern cycle completions (over a long period of time), we can now consider $P(r_a, t)$, $P(r_b, t)$, etc., where $P(r_a, t)$ is the probability that, after a sufficiently long time t, any single system of the ensemble has completed r_a *net* cycles in the + direction around cycle a, etc. Since t is large, r_a may be regarded as a continuous variable.

Over a long time interval, the completion of cycles of each kind (a, b, . . .) may be treated as an independent, one-dimensional biased walk with, for cycle a, a transition probability k_{a+} in the + direction and k_{a-} in the − direction, etc. Thus, r_a is the net number of steps of the walk in the + direction. As is well known, the (Fokker-Planck) differential equation in $P(r_a, t)$ (similarly for b, c, . . .) has the form

$$\frac{\partial P}{\partial t} = \frac{1}{2}(k_{a+} + k_{a-}) \frac{\partial^2 P}{\partial r_a^2} - (k_{a+} - k_{a-}) \frac{\partial P}{\partial r_a} \tag{49}$$

with the solution

$$P(r_a, t) = [2\pi \sigma_a^2(t)]^{-1/2} \exp\left\{ - \frac{[r_a - \bar{r}_a(t)]^2}{2\sigma_a^2(t)} \right\} \tag{50}$$

where the mean $\bar{r}_a$ and variance σ_a^2 of the Gaussian distribution in r_a are given by

$$\bar{r}_a(t) = (k_{a+} - k_{a-})t = \bar{J}_a t / N, \qquad \sigma_a^2(t) = (k_{a+} + k_{a-})t = (\bar{J}_{a+} + \bar{J}_{a-})t/N \tag{51}$$

The Gaussian distribution in r_a both moves ($\bar{r}_a$) and spreads (σ_a^2) with constant velocity.

Let $n_a(t)$ be the total number of a cycles, either a_+ or a_-, completed in time t. Since the frequency of occurrence of such cycles is just $k_{a+} + k_{a-}$, we have from eq 51b, $\sigma_a^2(t) = n_a(t)$. Thus, in terms of n_a rather than t

$$\bar{r}_a = (k_{a+} - k_{a-}) n_a / (k_{a+} + k_{a-}), \qquad \sigma_a^2 = n_a \tag{52}$$

As usual, the distribution gets *relatively* sharper as t and n_a increase: $\sigma_a / \bar{r}_a \sim n_a^{-1/2} \sim t^{-1/2}$.

At this point we digress to comment on our frequent mention of long time intervals. Suppose, in observing the stochastic behavior of a system that started originally in state j, that a cycle has just been completed and the system is in, say, state i, where it may be that $i \neq j$ (if the diagram has more than one cycle). Now the probability that the *next* cycle (starting from state i) is a_+, a_-, b_+ etc., depends on the "left over" sequence of states (≥ 1), starting with j and ending with i, that has not yet been used in a cycle (Hill and Chen, 1975). If we average over j (as we would for an ensemble of systems), and use long enough times, this "memory" effect will be averaged out, leading to the mean stochastic parameters already introduced: k_{a+}, k_{a-}, . . . , p_{a+}, p_{a-}, . . . , τ. Because of this and other complications when dealing with short time intervals, we have not written the discrete (master equation) version of eq 49.

When several independent random events contribute to the fluctuating quantity of interest, both mean values and variances are additive. Actually, eq 51 are examples of this (a_+ and a_- are independent). Another example is the consideration of an ensemble of N independent systems rather than a single system. This, in fact, corresponds to the experimental situation. Equations 49 and 50 apply also to the ensemble, where $t \rightarrow N\Delta t$ and $P(r_a, \Delta t)$ is in this case the probability that r_a is the net number of a cycles in the + direction completed in the whole ensemble in time Δt, with

$$\bar{r}_a = N(k_{a+} - k_{a-})\Delta t = \bar{J}_a \Delta t, \qquad \sigma_a^2 = N(k_{a+} + k_{a-})\Delta t = (\bar{J}_{a+} + \bar{J}_{a-})\Delta t \tag{53}$$

In effect, the cycle rate constants have become (for the ensemble) Nk_{a+}, Nk_{a-}, etc. Of course now $N\Delta t$ must be large, but Δt may be small.

Still another example of additivity occurs in relation to cases such as eq 26. For example, suppose either cycle a or cycle b transports one Na^+ across a membrane. Then $r_{Na} \equiv r_a + r_b$ and eq 50 holds for $P(r_{Na}, \Delta t)$, where

$$\bar{r}_{Na} = N(k_{a+} - k_{a-} + k_{b+} - k_{b-})\Delta t = (\bar{J}_a + \bar{J}_b)\Delta t \tag{54}$$

$$\sigma_{Na}^2 = N(k_{a+} + k_{a-} + k_{b+} + k_{b-})\Delta t = (\bar{J}_{a+} + \bar{J}_{a-} + \bar{J}_{b+} + \bar{J}_{b-})\Delta t$$

Recall that $\bar{J}_{a+}$, etc., are all positive.

Noise Power Spectrum. If, say, membrane transport of Na^+ by a large ensemble of N carriers, in eq 54, involved no other physical process than those already included in the biochemical cycle, then the noise in J_{Na} is simple shot noise and the power density spectrum $G(f)$, f = frequency, is a constant (Middleton, 1960):

$$G = 2(\bar{J}_{a+} + \bar{J}_{a-} + \bar{J}_{b+} + \bar{J}_{b-}) \tag{55}$$

However, this is an oversimplification not only because of the possibility of other physical processes but also because we have averaged out (see above) the "texture" of the stochastic behavior of the system in the frequency range of individual cycles and transitions. That is, roughly speaking, eq 55 applies only at lower than cycle frequencies (τ^{-1}).

Numerical Example. We extend here the example in

Figure 6, eq 36 and 40, and on the left side of Table I ($K = 2$, $A = 1$, $B = 1/16$). We have

$$k_{a+} = \bar{J}_{a+}/N = K^6/\Sigma$$
$$k_{a-} = \bar{J}_{a-}/N = 1/\Sigma \quad (56)$$
$$k_{b+} = \bar{J}_{b+}/N = AK^3(\ )/\Sigma$$

etc. Table II gives, on the left, numerical values for all the k's, and their net values, which are equal to $\bar{J}_a/N$, etc. (compare Table I, left side). The reciprocal of the sum of the k's is τ, the mean time between cycles. The cycle probabilities ($p_{a+} = \tau k_{a+}$, etc.) are on the right of Table II. Of all cycles, 91% are of type a+ or b+. The cycle rate constants (the k's) should be compared in magnitude with the individual transition rate constants (of order unity). In fact, it is easy to show (see below) that the mean time between individual transitions in this example is $\tau_{tr.} = 0.3188$, which is smaller than the mean time between cycles τ, by a factor of 12.70. To calculate $\tau_{tr.}$ we have used the facts that: the mean time $\tau_{tr.}^{(i)}$ in any state i (between transitions) is the reciprocal of the sum of the *outgoing* rate constants from state i; and $p_i \sim f_i \tau_{tr.}^{(i)}$, where p_i is the steady-state probability of state i and f_i is the fraction of all transitions that start from state i. The f_i can be found from the known values of the p_i and $\tau_{tr.}^{(i)}$. Then $\tau_{tr.} = \Sigma f_i \tau_{tr.}^{(i)}$.

Table II: Example: Cycle Kinetics, $A = 1$, $B = 1/16$.

$k_{a+} = \bar{J}_{a+}/N = 0.1198$	$p_{a+} = 0.4851$
Net = 0.1179	
$k_{a-} = \bar{J}_{a-}/N = 0.0019$	$p_{a-} = 0.0076$
$k_{b+} = \bar{J}_{b+}/N = 0.1048$	$p_{b+} = 0.4244$
Net = 0.1040	
$k_{b-} = \bar{J}_{b-}/N = 0.0008$	$p_{b-} = 0.0033$
$k_{c+} = \bar{J}_{c+}/N = 0.00655$	$p_{c+} = 0.0265$
Net = −0.00655	
$k_{c-} = \bar{J}_{c-}/N = 0.01310$	$p_{c-} = 0.0531$
Sum of k's = 0.2470, $\tau = 4.049$	

5. Models for Active Transport by NaK-ATPase

We shall not introduce any additional explicit models in this section because no really new principles arise—only further complexity. But a few general remarks may be useful.

The diagram may be rather complicated (see, for example, Stone, 1968; Hill, 1968). There are now three thermodynamic forces: $\Delta\mu_{Na}$, $\Delta\mu_K$ (defined as in eq 22), and $\Delta\mu_T$, where

$$\Delta\mu_T \equiv \mu_{ATP} - (\mu_{ADP} + \mu_P) \quad (57)$$

We have used extensively $\Delta\mu_T$ as a chemical force in the muscle diagram (Hill, 1974; Hill et al., 1975). See also section 2 which is basically similar. In the muscle diagram, for simplicity, we generally treated products as a single entity:

$$M + ATP \rightleftharpoons M\cdot ATP \rightleftharpoons M\cdot(ADP, P) \rightleftharpoons M + (ADP, P) \quad (58)$$

where M = myosin cross-bridge. Here it is likely that products are released sequentially (with ADP released very fast):

$$C + ATP \rightleftharpoons C\cdot ATP \rightleftharpoons C\cdot(ADP, P) \rightleftharpoons CP + ADP \rightleftharpoons C + ADP + P \quad (59)$$

where C = carrier. Thus the carrier may be phyosphorylated in several states of the diagram.

Since $\Delta\mu$ is defined as $\mu^{out} - \mu^{in}$ (eq 22) for both Na^+ and K^+, we have here

$$\Delta\mu_{Na} > 0,\ \Delta\mu_K < 0,\ \Delta\mu_T > 0 \quad (60)$$

The force $\Delta\mu_T$ is sufficient to drive both Na^+ and K^+ against these electrochemical gradients. That is, the mean net fluxes (out → in is taken as positive for Na^+ and K^+) are

$$\bar{J}_{Na} < 0,\ \bar{J}_K > 0,\ \bar{J}_T > 0 \quad (61)$$

where $\bar{J}_T$ is the mean net flux ATP → ADP + P, and

$$\bar{J}_T\Delta\mu_T > (-\bar{J}_{Na})\Delta\mu_{Na} + \bar{J}_K(-\Delta\mu_K) \quad (62)$$

All factors and products are positive in eq 62 (using the parentheses). The efficiency is

$$\eta = \frac{(-\bar{J}_{Na})\Delta\mu_{Na} + \bar{J}_K(-\Delta\mu_K)}{\bar{J}_T\Delta\mu_T} \quad 0 \le \eta \le 1 \quad (63)$$

The free energy levels of the individual states of the diagram are handled as in sections 1–3.

If there is only one important cycle (as in most current models of the NaK-ATPase system), there will be complete coupling between the three fluxes. In a one-cycle model in which one circuit transports one Na^+, one K^+, and splits one ATP, $-\bar{J}_{Na} = \bar{J}_K = \bar{J}_T$. But if, say, one circuit transports three Na^+, two K^+, and splits one ATP, $-(1/3)\bar{J}_{Na} = (1/2)\bar{J}_K = \bar{J}_T$. In the latter case

$$\eta = \frac{3\Delta\mu_{Na} + 2(-\Delta\mu_K)}{\Delta\mu_T} \quad (64)$$

If the Na^+ equilibrium potential is estimated to be 115 mV more positive than the membrane rest potential and the K^+ equilibrium potential is taken as 10 mV more negative than the rest potential, the numerator in eq 64 becomes $3 \times 2.65 + 2 \times 0.23 \simeq 8.41$ kcal mol^{-1}. If $\Delta\mu_T \simeq 12$ kcal mol^{-1}, the efficiency is about 70%. Other cycles in the diagram would "uncouple" the fluxes and reduce η (see section 3).

If there are multiple cycles in the diagram, Figure 8a would have to be extended to three dimensions to accommodate the three thermodynamic forces. In the special case of only one important cycle, the three-dimensional biased walk on the extended Figure 8a would degenerate into a one-dimensional walk (as along the line $\eta = \eta_{max}$ in Figure 8a).

References

Hill, T. L. (1960), Statistical Thermodynamics, Reading, Mass., Addison-Wesley.

Hill, T. L. (1963), Thermodynamics of Small Systems, Part I, New York, N.Y., W. A. Benjamin.

Hill, T. L. (1964), Thermodynamics of Small Systems, Part II, New York, N.Y., W. A. Benjamin.

Hill, T. L. (1966), *J. Theor. Biol. 10,* 442.

Hill, T. L. (1968), Thermodynamics for Chemists and Biologists, Reading, Mass., Addison-Wesley.

Hill, T. L. (1974), *Prog. Biophys. Mol. Biol. 28,* 267.

Hill, T. L. (1975), *Prog. Biophys. Mol. Biol. 29,* (in press).

Hill, T. L., and Chen, Y. (1975), *Proc. Natl. Acad. Sci. U.S.A.* (in press).

Hill, T. L., Eisenberg, E., Chen, Y., and Podolsky, R. J. (1975), *Biophys. J.* (in press).

King, E. L., and Altman, C. (1956), *J. Phys. Chem. 60,* 1375.

Mahler, H. R., and Cordes, E. H. (1971), Biological Chemistry, New York, N.Y., Harper and Row.

Middleton, D. (1960), Statistical Communication Theory, New York, N.Y., McGraw-Hill.

Stone, A. J. (1968), *Biochim. Biophys. Acta 150,* 578.